Contents lists available at ScienceDirect

Extreme Mechanics Letters

journal homepage: www.elsevier.com/locate/eml

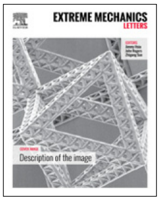

On the fragmentation of active material secondary particles in lithium ion battery cathodes induced by charge cycling

Guanhua Sun [a,b], Tan Sui [a], Bohang Song [a,1], Hong Zheng [b], Li Lu [c], Alexander M. Korsunsky [a,*]

[a] *Multi-Beam Laboratory for Engineering Microscopy (MBLEM), Department of Engineering Science, University of Oxford, Parks Road, Oxford OX1 3PJ, United Kingdom*

[b] *State Key Laboratory of Geomechanics and Geotechnical Engineering, Institute of Rock and Soil Mechanics, Chinese Academy of Sciences, Wuhan, Hubei 430071, China*

[c] *Department of Mechanical Engineering, National University of Singapore, Block EA#07-08, 9 Engineering Drive 1, Singapore 117575, Singapore*

HIGHLIGHTS

- Primary particle lattice strain due to Li^+ causes secondary particle cracking with charge cycling.
- Coupled electro-chemical-mechanical model reveals progressive polycrystal aggregate cracking.
- Discrete element method with cohesive crack modelling captures charge rate effects.

GRAPHICAL ABSTRACT

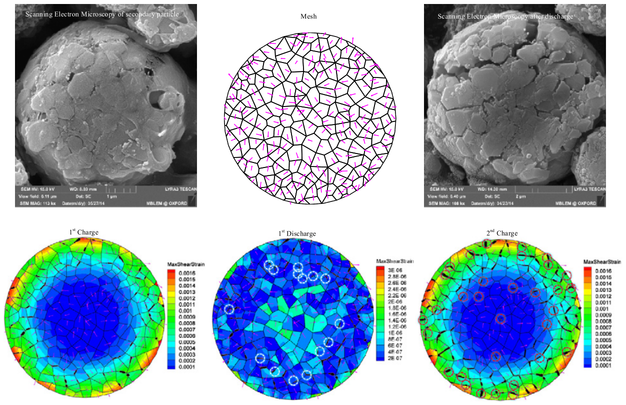

Fracture due to coupled electrochemical-mechanical process by charge cycling

ARTICLE INFO

Article history:
Received 7 January 2016
Received in revised form 14 March 2016
Accepted 22 March 2016
Available online xxxx

ABSTRACT

The loss of connectivity within battery electrodes due to mechanical failure by decohesion and fracture between primary grains that form spheroidal secondary particles is one of the principal mechanisms responsible for the widely observed and reported capacity fading. In this study we focus our attention on the elucidation, via combined analytical and numerical modeling, of the coupled electrochemical and mechanical processes that occur

---

[*] Corresponding author. Tel.: +44 18652 73043; fax: +44 18652 73010.
E-mail address: alexander.korsunsky@eng.ox.ac.uk (A.M. Korsunsky).

[1] Current address: University of Texas, Austin, USA.

http://dx.doi.org/10.1016/j.eml.2016.03.018

Please cite this article in press as: G. Sun, et al., On the fragmentation of active material secondary particles in lithium ion battery cathodes induced by charge cycling, Extreme Mechanics Letters (2016), http://dx.doi.org/10.1016/j.eml.2016.03.018

Keywords:
Li-ion battery cathode
Degradation
Capacity fading
Electrochemical–mechanical model
Fragmentation
Fracture

during lithiation and delithiation. We run sequential diffusion and deformation analyses of polycrystalline aggregate, formulate conditions for crack initiation at the interfaces between primary particles, and obtain predictions for the distributed damage within the secondary particle. The discrete element method with cohesive crack modeling is employed as the simulation tool. The conclusions that can be drawn from the analysis can be summarized as follows: (1) anisotropic expansion of primary particle crystallites due to Li^+ ion diffusion causes cracks to form at the interfaces and grain boundaries when stresses reach the cohesive strength limit; (2) Li^+ ion concentration and its gradients have influence on crack formation, distribution and density, with high charging and steep gradients promoting rupture; (3) anisotropic particle expansion/contraction promotes interfacial fracture; (4) new crack appear and existing cracks extend under cyclic charging conditions.

1. Introduction

It is well known that the loss of continuity and conductivity within battery electrodes caused by micro-scale fracture is one of the major causes for the degradation in Li-ion batteries [1–3]. Specific effects include the loss of electrical contact, isolation of active materials from the conductive matrix, and increased cell internal resistance [4]. Fracture also increases the exposure of active materials to the electrolyte, accelerating irreversible side reactions such as the formation of the solid–electrolyte interface, and leading to capacity fading [4].

The crack formation and damage evolution within secondary particles in battery electrodes have been addressed in many studies. Damage within the active material particles can be seen in the form of voiding, cracking and ultimate fragmentation [5]. Based on the energy release rate, the effects of particle size and charging rate on fracturing in an electrode particle were studied by Zhao et al. [6], who also predicted the critical fracture conditions. Woodford et al. constructed a map showing the safe parameter regimes against fracture, which depended on the C-rate (that describes the normalized charging rate of a cell and has units of h^{-1}), particle size and fracture toughness of the material [7]. Bhandakkar et al. calculated the critical electrode size to avoid crack nucleation in a cylindrical electrode particle [8]. Zhu et al. evaluated the effects of current density, particle size and particle aspect ratio on crack initiation by means of eXtended Finite Element Method XFEM [9]. These studies have revealed the critical conditions that determine whether a crack will grow or not [4]. Furthermore, Grantab et al. investigated the progressive propagation of a crack during cycling in a graphite particle [10] or in a silicon nanowire [11].

Local fractures have been experimentally observed in several cathode materials for Li-ion batteries [2,5,12–14]. An obvious cause of fracture in battery materials is high local micro-scale stress [9] that may arise during fabrication that usually involves compression to control the porosity of the cathode [15–18], or which may result from cell cycling throughout the life of a Li-ion battery due to the intercalation of lithium ions, as well as the phase transition within active materials [9].

Several models have been developed to determine the stress generated by lithium intercalation and deintercalation. In order to identify key mechanisms and relationships involved in stress generation in spherical particles, one-dimensional models have been developed [19,20]. Three-dimensional finite element simulations have also been employed to model the diffusion-induced stress in analogy with thermal stresses [21,22], and relationships have been put forward between stresses and parameters such as current density, voltage and particle size. Analytical expressions have been constructed to capture the stress evolution in spherical electrode particles under galvanostatic or potentiostatic conditions [23–25] in an attempt to determine which operating conditions are “safe” in terms of preventing cracking in electrodes. Stress generated in spherical particles that consider both diffusion and phase transition can be calculated analytically and used to predict fracture [25].

The objectives of the present work are:

(1) To model internal strains and stresses caused by Li^+ diffusion within secondary particles, and predict crack initiation at interfaces.
(2) To assess the influence of concentration gradients due to Li^+ diffusion on crack distribution.
(3) To assess the influence of crystal lattice expansion and contraction lithiation coefficients on secondary particle cracking, as a consequence of damage accumulation due to Li-ion induced strain and strain gradients.
(4) To explore cracks evolution due to cyclic charging.

2. Description of material and experimental observations

Scanning Electron Microscopy (SEM) imaging of secondary particles (Fig. 1), and 3D reconstruction of their shape using Focused Ion Beam (FIB) serial sectioning (Fig. 2) reveal that secondary particles of active material appear as disks in cross-section, and have spheroidal shape overall. The constituent primary particles (Fig. 1(b)) appear as “stacks” of approximately hexagonal platelets, or as crystallites with well-defined habit and facets. Within a well-formed secondary particle (Fig. 1(c)) these are well-bonded, without any significant gaps or cracks.

FIB-SEM serial sectioning has been used to reconstruct the evolution of the three-dimensional structure of Li-ion battery electrodes during extended cycling [5]. Fig. 2 provides a pseudo-3D image of the composite framework

Please cite this article in press as: G. Sun, et al., On the fragmentation of active material secondary particles in lithium ion battery cathodes induced by charge cycling, Extreme Mechanics Letters (2016), http://dx.doi.org/10.1016/j.eml.2016.03.018

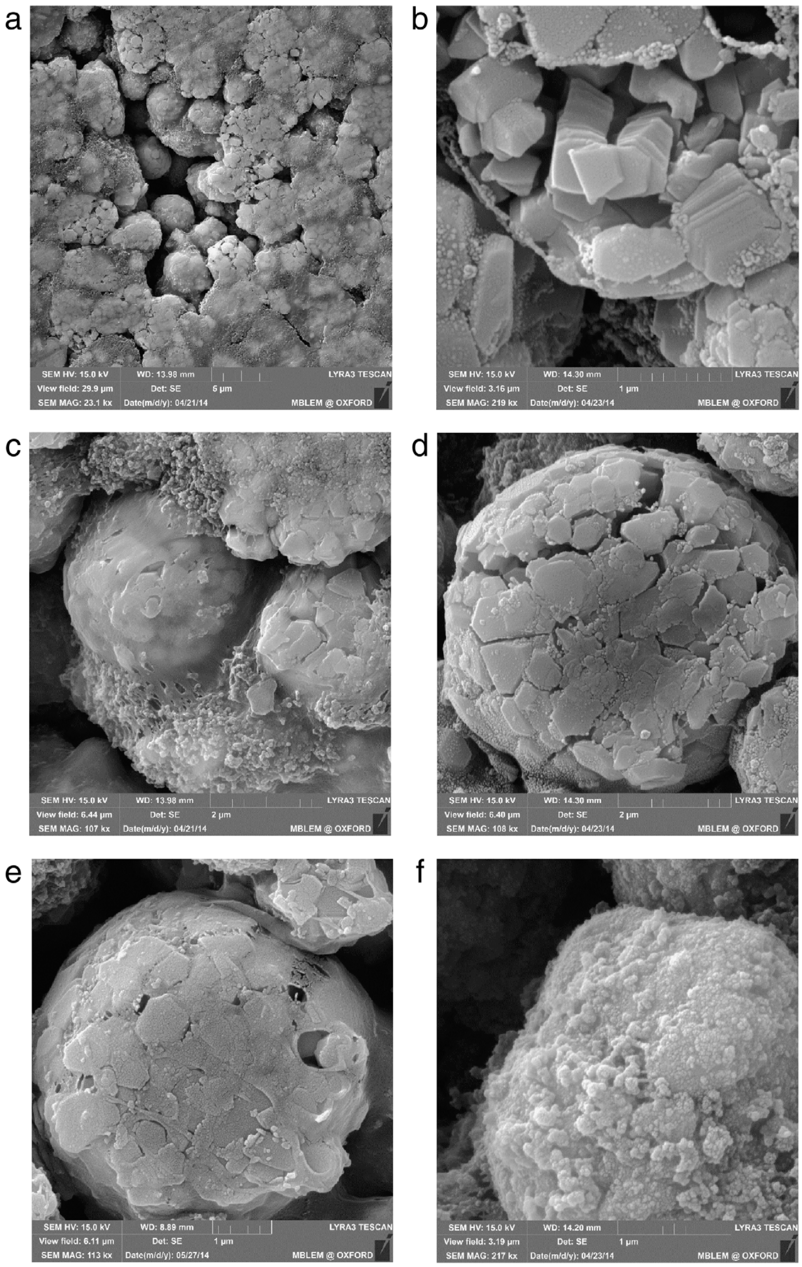

Fig. 1. (a) Overall low magnification view of Li battery Li-rich NMC cathode, showing agglomeration of spherical secondary particles. (b) High magnification view of second particle periphery revealing individual primary particles in the form of 'stacks' of hexagonal plates, and crystallites with well-defined facets. (c) Medium resolution imaging of the as-fabricated secondary particle (fully-discharged) prior to cycling, revealing well-bonded primary particles. (d) Secondary particle following first charge/discharge cycle revealing the presence of peripheral cracking. (e) Secondary particle following 15th cycle charging showing cracks closed due to lithiation-induced deformation. (f) Secondary particle after 50th cycle charging showing extensive fragmentation and amorphisation.

of spheroidal particles of active material contained within the polymer matrix. Damage within active material secondary particles takes the form of voiding, cracking and ultimate fragmentation. These observations of progressive cracking and fragmentation serve as the basis for the model proposed here.

The strain and strain gradients that arise in a secondary spheroidal particle due to Li^+ ion transient diffusion are identified as the driving force for particle fragmentation. Fig. 1(d) shows that already upon first charge/discharge cycle, gaps and cracks appear between primary particles. Subsequent charging and discharging takes the particle through a sequence of steps of crack nucleation and growth, followed by closure (perhaps accompanied by initiation and cracking at other interfaces), ultimately leading to profound fragmentation, primary particle diminution,

Please cite this article in press as: G. Sun, et al., On the fragmentation of active material secondary particles in lithium ion battery cathodes induced by charge cycling, Extreme Mechanics Letters (2016), http://dx.doi.org/10.1016/j.eml.2016.03.018

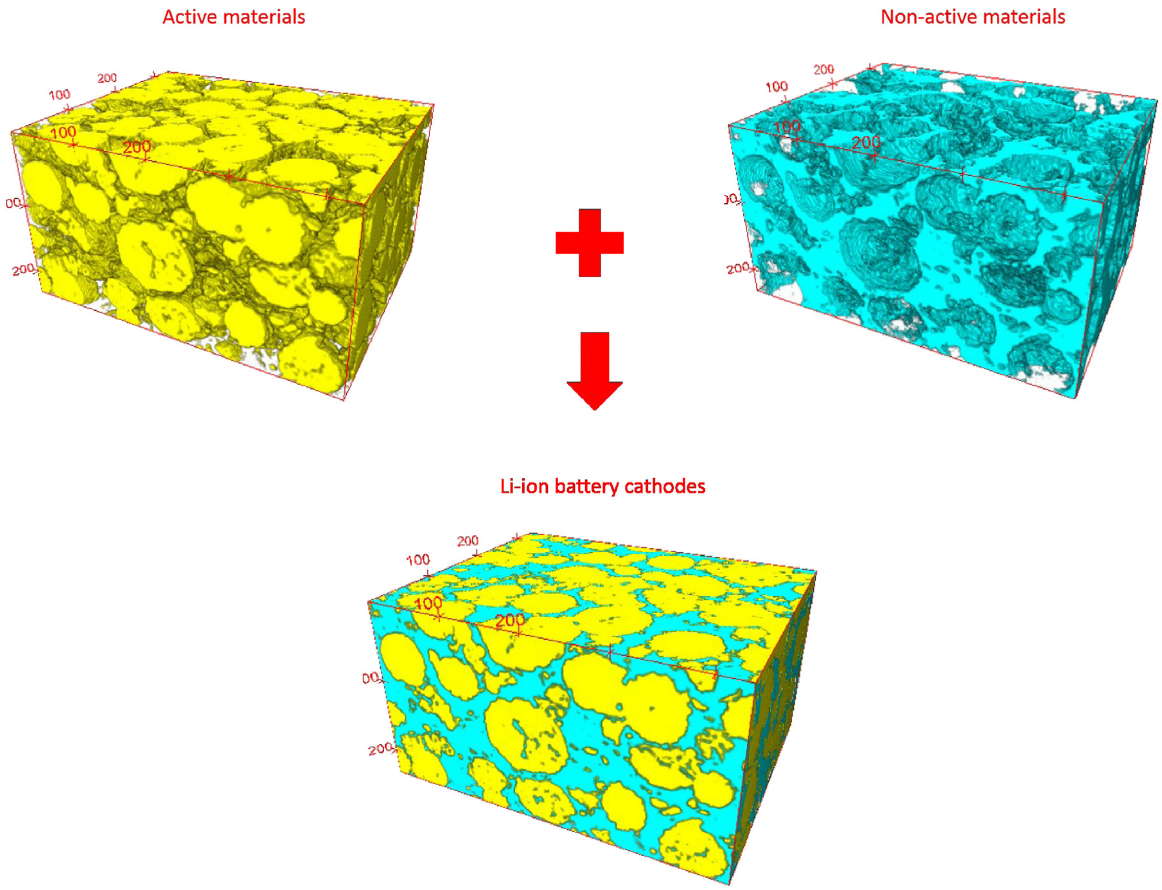

Fig. 2. FIB-SEM serial sectioning reconstructions of battery cathodes, represented as a composite framework of spheroidal particles of active material (top left image, in yellow) contained within the polymer matrix (top right, in light blue), and shown as a complete reconstruction below.

and amorphization, seen in Fig. 1(e) for a particle within the battery cathode after 15 cycles, and in Fig. 1(f) after 50 cycles.

The high magnification SEM image in Fig. 1(b) reveals the hexagonal habit platelets of oxides that can be clearly recognized in the small stack found to the bottom right of image center, and viewed at an aspect nearly parallel to the out-of-plane (c-axis) directions. Careful analysis of images reveals that particles are often composed of laminae ~50 nm in thickness. This discussion suggests significant anisotropy of thermal, electrochemical, mechanical and diffusional properties of primary particles between the basal plane and c-axis. It is surmised that their agglomerates are likely to experience significant internal strains and stresses due to electrochemical processes associated with Li ion intercalation and deintercalation. This observation is supported by the evidence from *in operando* synchrotron X-ray diffraction studies that reveal lattice parameter changes of the order of $\pm 1\%$ are apparent in the majority $LiMO_2$ ($M = $ Ni, Co, and/or Mn) rhomboheral phase with the $R\bar{3}m$ structure [26].

The above discussion provides a conceptual basis for continuum-based models of damage and degradation of secondary particles induced by lithiation and delithiation during charge cycling.

3. Modeling approach

The history of continuum mechanics knows numerous examples of simplified models that obviate the necessity of carrying our full 3D analysis of complex systems by proposing a simplification, such as the reduction to a much more tractable 2D description that allows fast parametric analysis, establishes the causal connections between system properties and behavior, etc. The present study is conducted in the same spirit. We recognize that the process of spherical secondary particle fragmentation upon charge cycling arises as a consequence of inhomogeneous and anisotropic expansion and shrinkage of constituent primary particles in the context of hoop constraint. For the purposes of the present consideration of the fundamental relationships between problem parameters we employ a simplified 2D model in which the secondary particle is represented by a right circular cylinder composed of multiple primary particles (grains) of random orientation. Two aspects of our approach should be made clear. (i) In reality, the polycrystalline particles of active material (secondary particles) have spherical shape. It is in order to provide

Please cite this article in press as: G. Sun, et al., On the fragmentation of active material secondary particles in lithium ion battery cathodes induced by charge cycling, Extreme Mechanics Letters (2016), http://dx.doi.org/10.1016/j.eml.2016.03.018

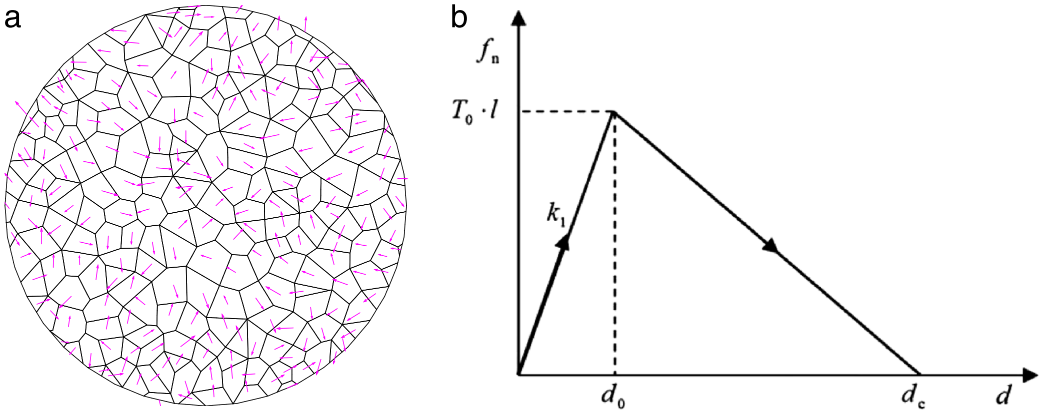

Fig. 3. (a) Schematic of the model of a spherical particle, consisting of 5676 nodes, 7816 elements and 225 grains. The *c*-axis orientation within each grain is indicated by arrows. (b) Relationship between the cohesive force and the displacement.

clear evidence of this fact that we wish to make use of microscopic images from our previous publications. (ii) It becomes apparent from these images is that in cross-section the particles appear as circular disks, so that the appropriate 2D approximation that might be considered suitable for simplified modeling is cylindrical, in combination with either plane stress or plane strain assumption.

A sequentially coupled model is employed to study the fracture inside a secondary particle. Only the crack initiation and propagation in the process of charging and discharging are chosen as the focus of the present study. Firstly, the concentration distribution of Li ions induced by transient diffusion is computed using an analytical approximate model. Secondly, the internal stress distribution within the particle is computed by considering the crystal lattice expansion and contraction due to (de)intercalation. The interface stresses obtained from this calculation are compared with the criterion for decohesion, and boundary fracture is introduced accordingly. The discrete element method is employed in this study to calculate the stress–strain fields, and to model grain boundary fracture.

3.1. Numerical simulation

For the purposes of this conceptual simulation, and to render the model readily tractable, 2D axial symmetry is assumed within the model (plane strain), as illustrated in Fig. 3(a), in which 5676 nodes, 7816 elements and 225 grains are consisted. In this study, the discrete element method [27] with the software UDEC [28] is employed to simulate the stress field and fracture behavior. Arrows indicate the randomly assigned *c*-axis direction within polygonal primary particles created by Voronoi tessellation. Young's modulus of active material is set to 280 GPa [5], and the secondary particle of diameter 2 μm is simulated.

3.2. Transient diffusion within a sphere

Consider the secondary particle of radius a initially fully saturated to normalized concentration $c_1 = 1$ throughout its volume. At time zero, the concentration is reduced to zero level $c_1 = 0$ at its surface and maintained at that level afterwards. The concentration with the sphere is governed by the transient diffusion equation:

$$\frac{\partial c}{\partial t} = D\nabla^2 c. \tag{1}$$

Rana et al. [29] gave the general solution of the equation with the method of separation of variables [30]. The complementary solution for the case of the sphere that is initially fully depleted of diffusant at $c = 0$, and undergoes inward diffusion (discharge) caused by the surface concentration raised to $c = 1$ at $t = 0$ is given by [31,32]:

$$c(r,t) = 1 + 2\sum_{n=0}^{\infty}(-1)^n \frac{a}{\pi n r} \times \exp\left(-\frac{\pi^2 n^2 D t}{a^2}\right)\sin\left(\frac{\pi n r}{a}\right). \tag{2}$$

Throughout the process of transient diffusion the concentration can be approximated well by a power law function [33] of normalized radius r/a and normalized diffusion time $\tau = Dt/a^2$:

$$c(r,t) = \left(\frac{r}{a}\right)^m = \left(\frac{r}{a}\right)^{0.655\tau^{-0.546}}. \tag{3}$$

3.3. Material properties and electrochemical–mechanical model

Assuming elastic isotropy, the stress–strain relation in the particle can be written as [24,34]

$$\varepsilon_{ij} = \frac{1}{E}\left[(1+\nu)\sigma_{ij} - \nu\sigma_{kk}\delta_{ij}\right] + c\beta_{ij} \tag{4}$$

where ε_{ij} are strain components, E is Young's modulus, ν is Poisson's ratio, σ_{ij} are stress components, δ_{ij} is the Kronecker delta, c is the Li-ion concentration and β_{ij} are the eigenstrain terms that represents the extreme values of anisotropic expansion and contraction of the crystal lattice due to the complete insertion or removal of the Li-ions. In

Please cite this article in press as: G. Sun, et al., On the fragmentation of active material secondary particles in lithium ion battery cathodes induced by charge cycling, Extreme Mechanics Letters (2016), http://dx.doi.org/10.1016/j.eml.2016.03.018

the present study this parameter in the crystal axes is set to ±1% (contraction of c-axis and expansion of a-axis upon lithiation), based on the evidence obtained by synchrotron X-ray diffraction [26].

Every primary particle within the model is identified by the orientation of its c-axis, as shown in Fig. 3(a). To transform the lattice expansion and contraction strains to the global coordinate system, the tensor transformation formula is used,

$$\beta_{i'j'} = \beta_{ij} n_{ii'} n_{jj'} \tag{5}$$

where $n_{ii'}$ and $n_{jj'}$ are directional cosines between the local coordinate system and the global coordinate system.

3.4. Fracture model

Cracks are assumed to initiate at interfaces between the primary particles when the corresponding stress component normal to the interface reaches the limiting cohesive strength of the boundary. The tension failure of the primary interface is simulated using cohesive crack model [35,36] suitable for the description of failure behavior in brittle materials. In this model a rising and falling cohesive force-opening relation is introduced according to the schematic in Fig. 3(b); the interface is supposed to have debonded once the cohesive force drops to zero. The normal cohesive force f_n as a function of separation is given by:

$$\begin{cases} f_n = k_1 d & (d < d_0) \\ f_n = k_1 d_0 \dfrac{d_c - d}{d_c - d_0} & (d_0 \le d < d_c) \end{cases} \tag{6}$$

where k_1 is the normal boundary stiffness; d is the relative displacement (interface opening) of the boundary; d_0 is the relative separation at maximum cohesive force equal to $T_0 l/k_1$, T_0 is the maximum tensile strength of the interface between the primary particles, l is the length of the interface in plane by assuming the crack length out of plane is equal to 1; d_c is the boundary separation at which the cohesive force drops to zero, determined as $2G_{IC}/T_0$, where G_{IC} is the fracture energy of Mode I crack.

3.5. Simulation scenarios

Three different simulation scenarios were considered, as described below.

(i) One step modeling

The first modeling scenario involves the transient diffusion solution for Li concentration $c(r)$ at normalized diffusion time $\tau = 0.03$. The corresponding concentration profile is applied directly without any interim steps. Two further cases of lithiation expansion coefficient are considered: the first case is *bipolar*, with the normal (c-axis) $\beta_n = -0.01$ and transverse (a-axis) $\beta_t = 0.01$; the second case is *unipolar*, $\beta_n = 0.02$ and $\beta_t = 0.0$.

(ii) Step-wise modeling

The second modeling scenario considered simulates the attainment of the same normalised diffusion time $\tau = 0.03$ that is however implemented in a step-wise fashion by following the evolution of Li concentration $c(r)$ at times. The total of five computational steps are considered ($\tau = 0.0001, 0.001, 0.01, 0.02, 0.03$).

(iii) Charging cycle

One case of charge cycling was simulated in the present study, namely, the bipolar case ($\beta_n = -0.01$, $\beta_t = 0.01$) using one-step scenario. The stages of the simulation were (i) charge to $\tau = 0.03$ (2) discharge to $\tau = 0.03$ using the configuration inherited from the previous step, and (3) repeated charge to $\tau = 0.03$ using the configuration inherited from the previous step.

4. Results and discussion

The results of "one step modeling" for both *bipolar* and *unipolar* cases are shown in the upper and lower rows of Fig. 4, with the left column showing the maximum shear strain (difference between principal strains), and the right column showing the first principal stress.

The results of "step-wise modeling" are presented in Fig. 5. Three time steps ($\tau = 0.0001, 0.01, 0.03$) illustrate the snapshots of the maximum shear strain and maximum principal stress within the secondary particle throughout the diffusion process. In addition, the c-axis lattice directions and crack locations are also represented, as per Figure caption.

The results of "charging cycles" are shown in Fig. 6. Fig. 6(a) is the contour of maximum shear strain and crack distribution after 1st charge, and Fig. 6(b) shows the corresponding contour of maximum principal stress. Fig. 6(c) represents the contour of maximum shear strain and cracks in the discharged condition, and Fig. 6(d) is the corresponding contour of maximum principal stress. Finally, Fig. 6(e) shows the contour of maximum shear strain and cracking after 2nd re-charge, and Fig. 6(f) is the corresponding contour of maximum principal stress.

4.1. The influence of lithiation expansion coefficient on crack formation

The two cases of the lithiation expansion coefficient considered in the simulation turn out to have a prominent effect on secondary particle fragmentation. The first case corresponding to *bipolar* expansion/contraction, $\beta_n = -0.01$ and $\beta_t = 0.01$, corresponds to the lattice shrinking in the c-axis direction upon lithiation, but expanding in the transverse direction (a-axis). The results are shown in Fig. 4(a–b), and can be compared with Fig. 4(c–d) showing the results for the *unipolar* assumption ($\beta_n = 0.02$ and $\beta_t = 0$).

It is apparent that more cracking is observed in the first case of *bipolar* expansion/contraction. The clear reason for this is the generation of tensile stress at interfaces between primary particles due to contraction, promoting rupture of interfaces.

4.2. The influence of diffusion gradient on crack formation

Interface rupture occurs most readily in the region of high concentration gradient at the periphery of the secondary particle. For an isolated secondary particle in

Please cite this article in press as: G. Sun, et al., On the fragmentation of active material secondary particles in lithium ion battery cathodes induced by charge cycling, Extreme Mechanics Letters (2016), http://dx.doi.org/10.1016/j.eml.2016.03.018

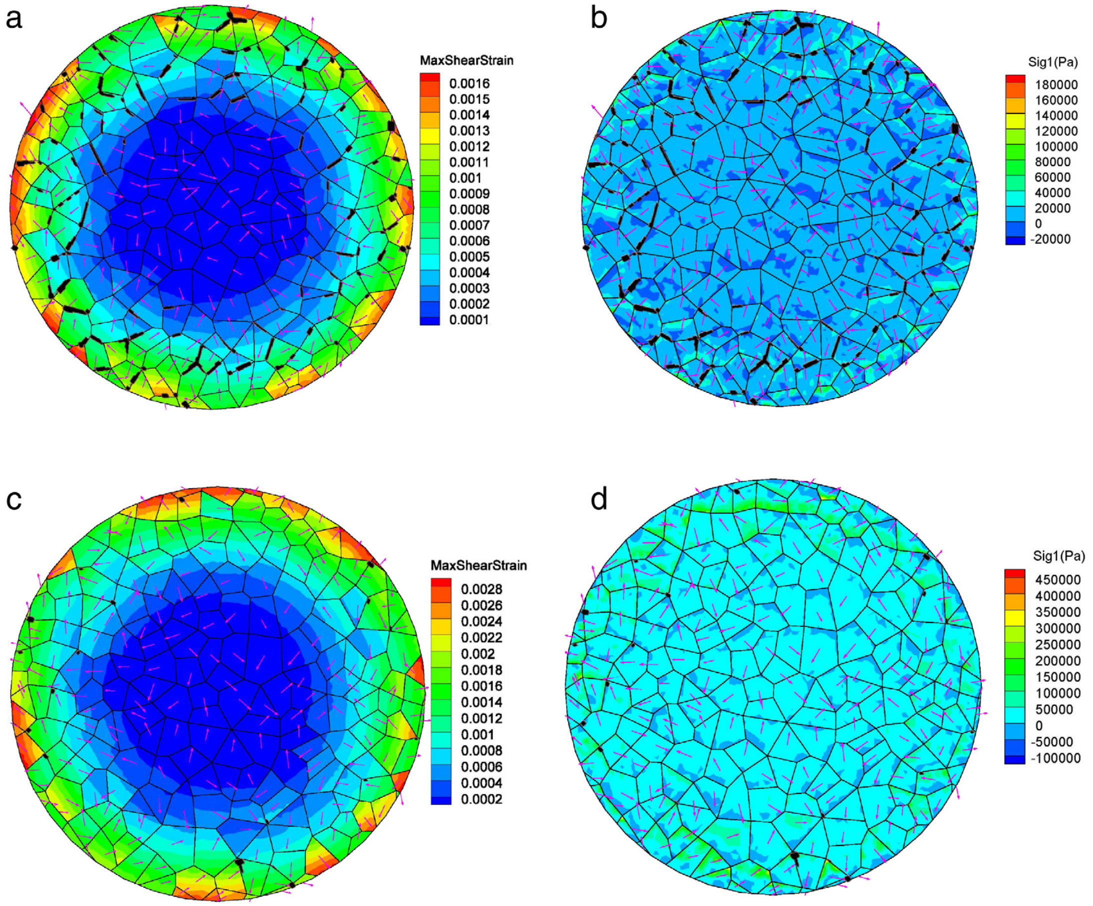

Fig. 4. Single step simulation of the consequences of diffusion at the normalised diffusion time $\tau = 0.03$: left column, (a) and (c) maximum shear strain distribution (proportional to the difference between principal strains); right column, (b) and (d) the most positive principal stress. Lithiation expansion coefficients are *bipolar* ($\beta_n = -0.01$, $\beta_t = 0.01$) for (a) and (b), the upper row; and *unipolar* ($\beta_n = 0.02$, $\beta_t = 0.0$) for (c) and (d), the bottom row.

the electrolyte, the lithium concentration distribution is isotropic with the lowest concentration gradient maintained at the particle core. The gradient of lithium concentration is large in the early stages of diffusion upon charging and discharging. As diffusion progresses from particle surface to its core, cracking also progresses inward.

4.3. Influence of progressive diffusion on crack formation and distribution

The two simulation scenarios of crack initiation due to transient diffusion further highlight the importance of strain gradients due to lithiation for causing fragmentation. In the first scenario (one-step simulation of transient diffusion to $\tau = 0.03$), Fig. 4, the extent of cracking is greater than that in Fig. 5, where the step-wise process of damage accumulation is shown for $\tau = 0.0001, 0.01, 0.03$.

Although the difference between the overall strain and stress distributions is small between the two cases, the extent of cracking is lower in the step-wise scenario. That is to say, in the scenario of transient diffusion the distribution of cracks initiation is extensive, but sparse. On the other hand, in the step-wise scenario the distribution of cracks is denser, but is more localised. The reason for this is that crack initiation that occurs in earlier steps causes stress concentration and subsequent crack propagation in subsequent steps. For example, Fig. 5(e) shows a major (labeled Crack I) that was initiated in the first step, and propagated in subsequent steps. The fracture labeled Crack II is freshly appeared in the final step of the simulation, and is associated with the influence of Crack I. This highlights the importance of capturing the damage accumulation mechanisms in order to capture its correct evolution. Thus, transient diffusion will result in more cracks initiated but a “continuous” charging case will result in more crack propagation. The reason for this is the difference between crack initiation and propagation, both of which are affected by the load path. Transient diffusion results in steep gradients and sudden loading; whereas continuous charging leads to cumulative loading. In the case of abrupt loading, the region where interfacial defects experience stress concentration is extensive. The final distribution of stress concentration and the crack distribution are affected by the pre-existing cracks and their propagation in the course of cumulative loading.

Our model demonstrates the “avalanche” nature of damage evolution in the active material particles due to charge cycling: simply applying the concentration map of Li ions obtained from the solutions of the diffusion equation at the final charge state leads to significantly

Please cite this article in press as: G. Sun, et al., On the fragmentation of active material secondary particles in lithium ion battery cathodes induced by charge cycling, Extreme Mechanics Letters (2016), http://dx.doi.org/10.1016/j.eml.2016.03.018

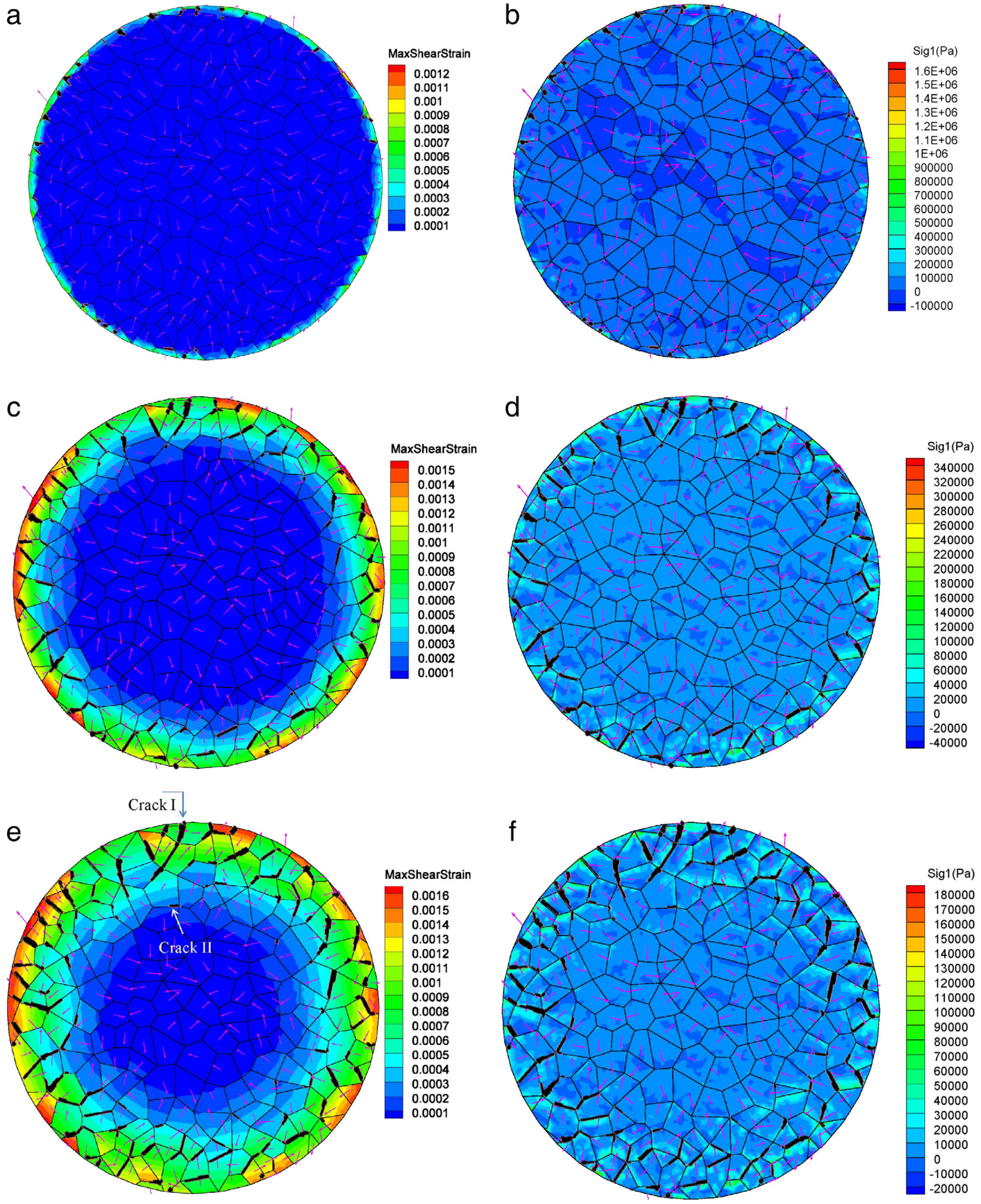

Fig. 5. Incremental (time-stepping) simulation of the consequences of lithiation: (a) maximum shear strain at $\tau = 0.0001$; (b) the most positive principal stress at $\tau = 0.0001$; (c) maximum shear strain at $\tau = 0.01$; (d) most positive principal stress at $\tau = 0.01$; (e) maximum shear strain at $\tau = 0.03$; (f) most positive principal stress at $\tau = 0.03$. Lithiation expansion coefficients are assumed to be ($\beta_n = -0.01$, $\beta_t = 0.01$). Arrows indicate the direction of c-axis within each primary particle.

smaller damage than results from a sequence of small steps following the evolution of Li^+ ion concentration. This is one of the fundamental results that we wish to present: the modification of particles structure due to cracking, even in the absence of diffusion gradients and Li^+ ion pile-ups that it creates, already couples into the mechanical fields (stresses and strains) in a way that promotes further particle fragmentation, accelerating the damage cascade that leads to battery capacity fading.

4.4. The evolution of crack formation due to charge cycling

The following observations can be made on the observed fragmentation. Firstly, the most significant extent

Please cite this article in press as: G. Sun, et al., On the fragmentation of active material secondary particles in lithium ion battery cathodes induced by charge cycling, Extreme Mechanics Letters (2016), http://dx.doi.org/10.1016/j.eml.2016.03.018

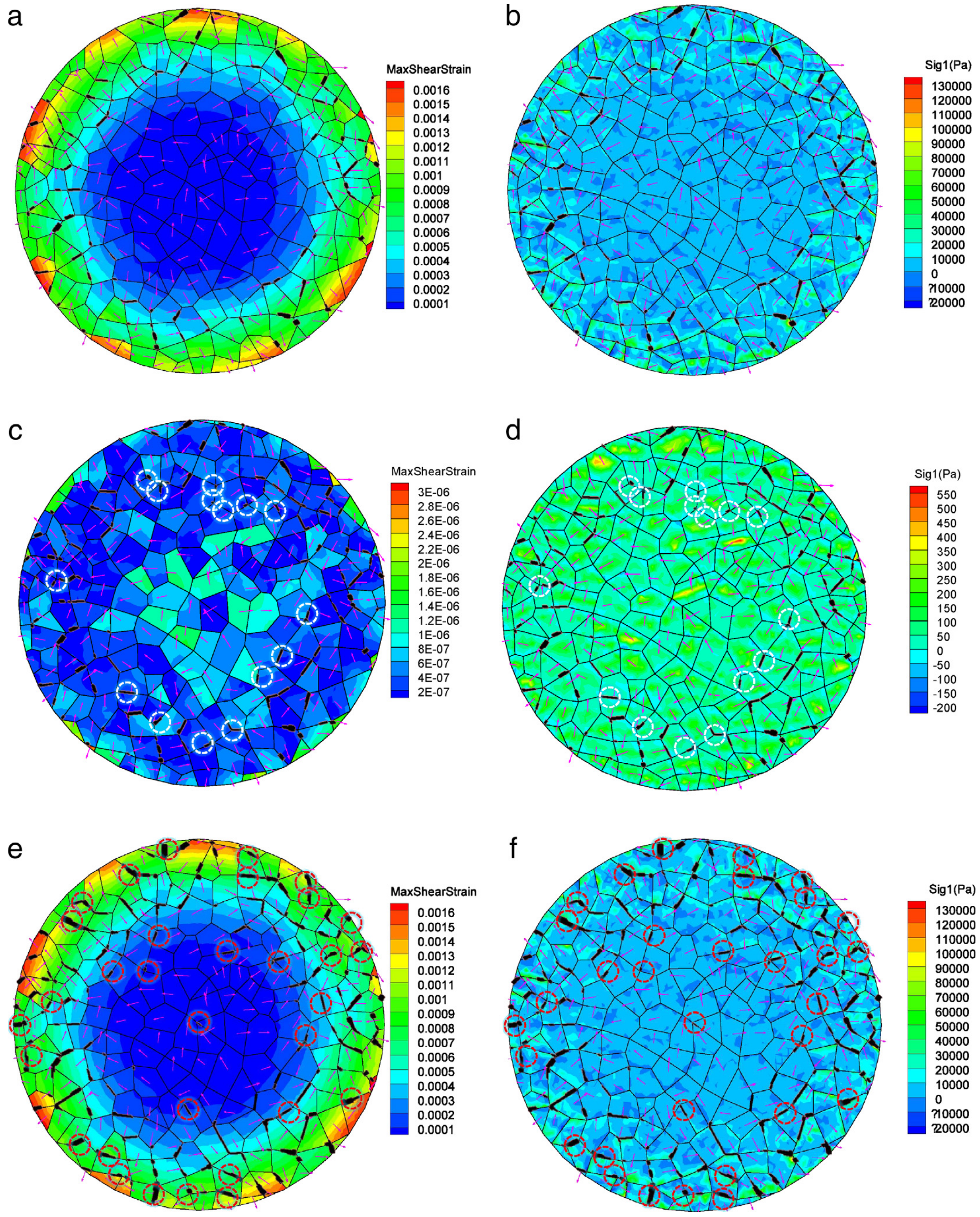

Fig. 6. Crack evolution during charge cycling: (a) maximum shear strain and (b) most positive principal stress after initial charging; (c) maximum shear strain, and (d) most positive principal stress after 1st discharging; (e) maximum shear strain and (f) most positive principal stress after 2nd re-charge. Locations of progressive damage due to cycling are circled.

of cracking in terms of its depth from the particle surface and towards its core occurs upon first charge. Subsequent rupture due to discharge and re-charge promotes further opening of the interfaces between primary particles that occurs both upon discharging and re-charging, indicating that both stages of the process are damaging. The cracks that appeared anew during subsequent cycling are indicated by the red dotted circles in Fig. 6. Pre-existing cracks from the previous process stage undergo extension during subsequent cycling.

These findings are consistent with the electrochemical observations of Li-ion battery cycling that indicate significant capacity loss during first cycling, followed by the much more gradual fading during subsequent cycling.

Please cite this article in press as: G. Sun, et al., On the fragmentation of active material secondary particles in lithium ion battery cathodes induced by charge cycling, Extreme Mechanics Letters (2016), http://dx.doi.org/10.1016/j.eml.2016.03.018

5. Conclusion

In this study, crack initiation and propagation at the interfaces between the primary particles in a secondary particle of active material within Li-ion battery cathode were simulated by discrete element method with the help of cohesive crack model.

The following conclusions are drawn from the analyses of the results:

(1) Diffusion of Li^+ ions causes lattice expansion and contraction that leads to crack formation at the interfaces between primary particles caused by the exhaustion of cohesive strength.

(2) The diffusion scenario considered affects the crack distribution that arises, with the interfaces being more easily ruptured due to the accumulation of damage from previous steps involving high concentration gradients.

(3) The assumption of *bipolar* expansion/contraction of primary particles due to lithiation leads to greater extent of damage due to the generation of tensile stresses.

(4) Damage accumulation during subsequent cycling manifests itself in new cracks appearing upon discharge and re-charge, highlighting the importance of both initial and cyclic damage.

Acknowledgments

Alexander M. Korsunsky acknowledges funding received for MBLEM laboratory at Oxford through EU FP7 project iSTRESS (604646), and access to the facilities at the Research Complex at Harwell (RCaH), under the Centre for In situ Processing Studies (CIPS). The authors have declared no conflict of interest.

References

[1] R.A. Huggins, W.D. Nix, Decrepitation model for capacity loss during cycling of alloys in rechargeable electrochemical systems, Ionics 6 (2000) 57–63.

[2] D. Wang, X. Wu, Z. Wang, L. Chen, Cracking causing cyclic instability of $LiFePO_4$ cathode material, J. Power Sources 140 (2005) 125–128.

[3] H.-L. Zhang, F. Li, C. Liu, J. Tan, H.-M. Cheng, New insight into the solid electrolyte interphase with use of a focused ion beam, J. Phys. Chem. B 109 (2005) 22205–22211.

[4] S. Lee, J. Yang, W. Lu, Debonding at the interface between active particles and PVDF binder in Li-ion batteries, Extreme Mech. Lett. 6 (2016) 37–44.

[5] B. Song, T. Sui, S. Ying, L. Li, L. Lu, A.M. Korsunsky, Nano-structural changes in Li-ion battery cathodes during cycling revealed by FIB-SEM serial sectioning tomography, J. Mater. Chem. A 3 (2015) 18171.

[6] K. Zhao, M. Pharr, J.J. Vlassak, Z. Suo, Fracture of electrodes in lithium-ion batteries caused by fast charging, J. Appl. Phys. 108 (2010) 073517.

[7] W.H. Woodford, Y.-M. Chiang, W.C. Carter, Electrochemical shock of intercalation electrodes: A fracture mechanics analysis, J. Electrochem. Soc. 157 (2010) A1052–A1059.

[8] T.K. Bhandakkar, H. Gao, Cohesive modeling of crack nucleation in a cylindrical electrode under axisymmetric diffusion induced stresses, Internat. J. Solids Struct. 48 (2011) 2304–2309.

[9] M. Zhu, J. Park, A.M. Sastry, Fracture analysis of the cathode in Liion batteries: A simulation study, J. Electrochem. Soc. 159 (2012) A492–A498.

[10] R. Grantab, V.B. Shenoy, Location- and orientation-dependent progressive crack propagation in cylindrical graphite electrode particles, J. Electrochem. Soc. 158 (2011) A948–A954.

[11] R. Grantab, V.B. Shenoy, Pressure-gradient dependent diffusion and crack propagation in lithiated silicon nanowires, J. Electrochem. Soc. 159 (2012) A584–A591.

[12] M.-R. Lim, W.-I. Cho, K.-B. Kim, Preparation and characterization of gold-codeposited LiMn204 electrodes, J. Power Sources 92 (2001) 168–176.

[13] H. Wang, Y.-I. Jang, B. Huang, D.R. Sadoway, Y.-M. Chiang, TEM study of electrochemical cycling-induced damage and disorder in $LiCoO_2$ cathodes for rechargeable lithium batteries, J. Electrochem. Soc. 146 (1999) 473–480.

[14] T. Li, B. Song, L. Lu, K. Zeng, Voltage induced electrochemical reactions in the single lithium-rich layer-oxide nanoparticles, Phys. Chem. Chem. Phys. 17 (2015) 10257–10264.

[15] K.A. Striebel, A. Sierra, J. Shim, C.-W. Wang, A.M. Sastry, The effect of compression on natural graphite anode performance and matrix conductivity, J. Power Sources 134 (2004) 241–251.

[16] C.-W. Wang, Y.-B. Yi, A.M. Sastry, J. Shim, K.A. Striebel, Particle compression and conductivity in Li-Ion anodes with graphite additives, J. Electrochem. Soc. 151 (2004) A1489–A1498.

[17] Y.-B. Yi, C.-W. Wang, A.M. Sastry, Compression of packed particulate systems: simulations and experiments in graphitic Li-ion anodes, ASME J. Eng. Mater. Technol. 128 (2006) 73–80.

[18] T. Sui, B. Song, J. Dluhos, L. Lu, A.M. Korsunsky, Nanoscale chemical mapping of Li-ion battery cathode material by FIB-SEM and TOF-SIMS multi-modal microscopy, Nano Energy 17 (2015) 254–260.

[19] K. Zaghib, J. Shim, A. Guerfi, P. Charest, K.A. Striebel, Effect of carbon source as additives in $LiFePO_4$ as positive electrode for lithium-ion batteries, Electrochem. Solid-State Lett. 8 (2005) A207–A210.

[20] J. Christensen, J. Newman, Stress generation and fracture in lithium insertion materials, J. Solid State Electrochem. 10 (2006) 293–319.

[21] X. Zhang, W. Shyy, A.M. Sastry, Numerical simulation of intercalation-induced stress in Li-ion battery electrode particles, J. Electrochem. Soc. 154 (2007) A910–A916.

[22] X. Zhang, A.M. Sastry, W. Shyy, Intercalation-induced stress and heat generation within single lithium-ion battery cathode, J. Electrochem. Soc. 155 (2008) A542–A552.

[23] Y.-T. Cheng, M.W. Verbrugge, The influence of surface mechanics on diffusion induced stresses within spherical nanoparticles, J. Appl. Phys. 104 (2008) 083521.

[24] Y.-T. Cheng, M.W. Verbrugge, Evolution of stress within a spherical insertion electrode particle under potentiostatic and galvanostatic operation, J. Power Sources 190 (2009) 453–460.

[25] Y.-T. Cheng, M.W. Verbrugge, Diffusion-Induced stress, interfacial charge transfer, and criteria for avoiding crack initiation of electrode particles, J. Electrochem. Soc. 157 (2010) A508–A516.

[26] B. Song, S.J. Day, T. Sui, L. Lu, C.C. Tang, A.M. Korsunsky, Mitigated phase transition during first cycle of a Li-rich layered cathode studied by in operando synchrotron X-ray powder diffraction, Phys. Chem. Chem. Phys. 18 (6) (2016) 4745–4752. http://dx.doi.org/10.1039/c5cp04801j.

[27] P.A. Cundall, A Computer Model for Simulating Progressive Large Scale Movements in Blocky Rock Systems, in: Proceedings of the Symposium of the International Society of Rock Mechanics (Nancy, France), vol. 1, 1971, Paper No. II-8.

[28] P.A. Cundall, R.D. Hart, Development of generalized 2-D and 3-D distinct element programs for modeling jointed rock, Itasca Consulting Group; U.S. Army Corps of Engineers (1985) Misc. Paper SL-85-1.

[29] J. Rana, M. Stan, R. Kloepsch, J. Li, G. Schumacher, E. Welter, et al., Structural changes in Li2MnO3 cathode material for Li-ion batteries, Adv. Energy Mater. 4 (2014) 1300998.

[30] A.N. Tikhonov, A.A. Samarskii, Equations of Mathematical Physics, Dover, 2011.

[31] J. Park, W. Lu, A.M. Sastry, Numerical simulation of stress evolution in lithium manganese dioxide particles due to coupled phase transition and intercalation, J. Electrochem. Soc. 158 (2011) A201–A206.

[32] X. Zhang, W. Shyy, A. Marie Sastry, Numerical simulation of intercalation-induced stress in Li-ion battery electrode particles, J. Electrochem. Soc. 154 (2007) A910–A916.

[33] A.M. Korsunsky, T. Sui, B. Song, Explicit formulae for the internal stress in spherical particles of active material within lithium ion battery cathodes during charging and discharging, Mater. Des. 69 (2015) 247–252.

[34] R. Deshpande, Y.T. Cheng, M.W. Verbrugge, Modeling diffusion-induced stress in nanowire electrode structures, J. Power Sources 195 (2010) 5081–5088.

[35] A. Hillerborg, M. Modéer, P.-E. Petersson, Analysis of crack formation and crack growth in concrete by means of fracture mechanics and finite elements, Cem. Concr. Res. 6 (1976) 773–781.

[36] Z.H. Jin, C.T. Sun, Cohesive zone modeling of interface fracture inelastic bimaterials, Eng. Fract. Mech. 72 (2005) 1805–1817.

Please cite this article in press as: G. Sun, et al., On the fragmentation of active material secondary particles in lithium ion battery cathodes induced by charge cycling, Extreme Mechanics Letters (2016), http://dx.doi.org/10.1016/j.eml.2016.03.018